



Volcanic SO₂ and SiF₄ visualization using 2-D thermal emission spectroscopy – Part 1: Slant-columns and their ratios

W. Stremme¹, A. Krueger^{1,2}, R. Harig², and M. Grutter¹

¹Centro de Ciencias de la Atmósfera, Universidad Nacional Autónoma de México, Mexico City, Mexico

²Technische Universität Hamburg-Harburg, Hamburg, Germany

Correspondence to: M. Grutter (grutter@unam.mx)

Received: 26 August 2011 – Published in Atmos. Meas. Tech. Discuss.: 12 September 2011

Revised: 16 December 2011 – Accepted: 23 January 2012 – Published: 2 February 2012

Abstract. The composition and emission rates of volcanic gas plumes provide insight of the geologic internal activity, atmospheric chemistry, aerosol formation and radiative processes around it. Observations are necessary for public security and the aviation industry. Ground-based thermal emission infrared spectroscopy, which uses the radiation of the volcanic gas itself, allows for continuously monitoring during day and night from a safe distance. We present measurements on Popocatepetl volcano based on thermal emission spectroscopy during different campaigns between 2006–2009 using a Scanning Infrared Gas Imaging System (SIGIS). The experimental set-up, measurement geometries and analytical algorithms are described. The equipment was operated from a safe distance of 12 km from the volcano at two different spectral resolutions: 0.5 and 4 cm⁻¹. The 2-dimensional scanning capability of the instrument allows for an on-line visualization of the volcanic SO₂ plume and its animation. SiF₄ was also identified in the infrared spectra recorded at both resolutions. The SiF₄/SO₂ molecular ratio can be calculated from each image and used as a highly useful parameter to follow changes in volcanic activity. A small Vulcanian eruption was monitored during the night of 16 to 17 November 2008 and strong ash emission together with a pronounced SO₂ cloud was registered around 01:00 a.m. LST (Local Standard Time). Enhanced SiF₄/SO₂ ratios were observed before and after the eruption. A validation of the results from thermal emission measurements with those from absorption spectra of the moon taken at the same time, as well as an error analysis, are presented. The inferred propagation speed from sequential images is used in a subsequent paper (Part 2) to calculate the emission rates at different distances from the crater.

1 Introduction

Volcanoes are known to emit large amounts of gases into the atmosphere and contribute with 10–15% of the global anthropogenic sulphur emissions (Halmer, 2002). The gas composition of these volcanic plumes are not well understood and differ for each volcano (Aiuppa, 2009). SO₂ from volcanoes has been detected by remote sensing methods both from the ground and from space. Its strong absorptions in the UV have been widely used by COSPEC (CORrelation SPECtrometer) and now more frequently by DOAS (Differential Optical Absorption Spectrometer) instruments to monitor its fluxes. Satellite-based instruments such as the SCHIAMACHY (SCanning Imaging Absorption Spectrometer for Atmospheric Cartography) and OMI (Ozone Monitoring Instrument), have also been successful in detecting volcanic plumes from space. In the infrared, global monitoring by thermal emission measurements is now possible by sounders with enough spectral resolution such as the TES (Tropospheric Emission Spectrometer) and IASI (Infrared Atmospheric Sounding Interferometer) instruments (Clarisse et al., 2008). From the ground, infrared studies of the volcanic plume composition have mostly used the solar absorption technique but also open-path and thermal emission FTIR spectroscopy.

Fourier Transform Infrared (FTIR) spectroscopy from the ground has been applied in vulcanology for the last two decades (Notsu et al., 1993; Mori et al., 1993; Francis et al., 1996, 1998; Love et al., 1998; Burton et al., 2001; Goff et al., 2001; Duffell et al., 2001) and many more as for example the recent measurements on Popocatepetl by Grutter et al. (2008) and Stremme et al. (2011). Passive spectroscopy works

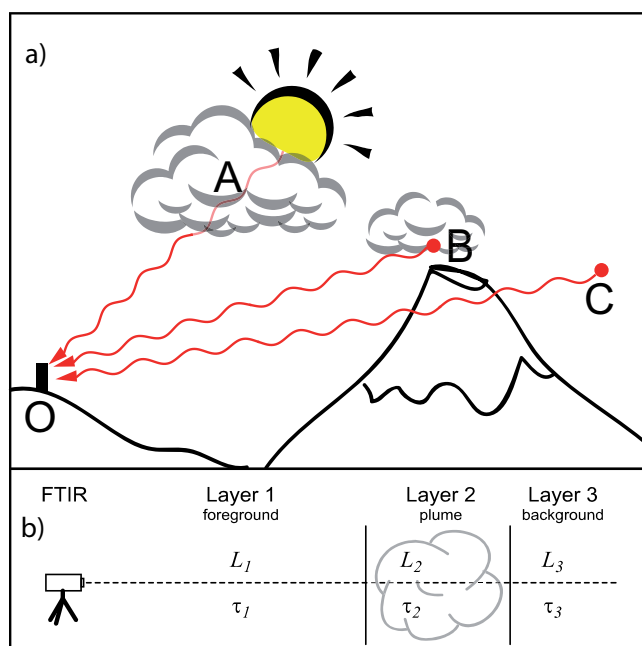


Fig. 1. (a) Different measurement geometries in the infrared using (A) solar/lunar absorption spectroscopy, (B, C) thermal emission spectroscopy at and beside the plume, respectively. SO_2 from Popocatépetl can readily be detected from thermal IR spectra and imaged by performing 2-D scans around the crater. A plume-sky difference (C–B) was used to analyze the weak SiF_4 signal and cope with the strong interferences. (b) Sketch of the three layers (background, plume and foreground) used in the forward model to simulate the spectra.

without controlling the radiation source and can be further distinguished in (A) absorption spectroscopy, which uses the sun, moon or hot rocks as light source and (B) thermal emission spectroscopy, using the radiation emitted by the target gas itself, which acts therefore as the light source. These geometries are depicted in the sketch provided in Fig. 1. While absorption spectroscopy needs the special condition that source, plume and sensor are in one line, thermal emission spectroscopy only requires a free sight of the plume. However, for a quantitative analysis of the gases, an accurate radiometric calibration is needed and the temperature (T -profile) along the line-of sight of the background, plume and foreground should be known or well estimated. A measurement along the direction C shown in Fig. 1, which is at the same elevation but barely missing the plume up-wind, as will be shown in this work, can aid in the analysis significantly.

According to our knowledge thermal emission spectroscopy to characterize volcanic emissions was applied for the first time in 1996 by Love et al. (1998, 2000) and Goff et al. (2001). From thermal emission spectroscopy, SO_2 , SiF_4 , H_2O , CO_2 (Goff et al., 2001) and even HCl (Love et al., 2000) have been determined in volcanic gas plumes. However, good H_2O and CO_2 results have proven to be

difficult to obtain because of their high atmospheric background. SiF_4 in volcanic gas was first detected by Francis et al. (1996) at Vulcano, which is a volcano on an Italian island, and the largest relative SiF_4 content was found at Satsuma-Iwojima volcano, Japan (Mori et al., 2002). Love et al. (1998) suggested that the increasing SiF_4 content measured in Popocatépetl might be related with the Vulcanian-type eruptions measured then and the molecular ratio of SiF_4 to SO_2 (SiF_4/SO_2) is thought to be an indicator of explosive activity (McGonigle, 2005). In a recent work, solar absorption measurements of Popocatépetl during an explosion and quiescent degassing showed a systematic difference in the HCl/SO_2 , HF/SO_2 and SiF_4/HF molecular ratios (Stremme et al., 2011). It was suggested that SO_2/HF ratios change and increase in explosions due to presence of gas originated from fresh magma from the depth, while SiF_4/HF ratios can increase due to a cooling of the stored gas near the surface.

In this work we present measurements of the thermal volcanic-plume radiation with a fully automated Scanning Infrared Gas Imaging System (Harig et al., 2005) and new retrieval strategies which allow for simultaneous monitoring of SO_2 and SiF_4 . As the determined slant columns are captured in two dimensional images, each scan or plume snapshot produces an average molecular ratio (SiF_4/SO_2) with a statistical measure of its significance. This parameter can be used to monitor changes in gas composition day and night, and possibly used as surveillance for future eruptive events. As example the results from a explosive event on the night of 16 to 17 November 2008 are presented. The propagation velocity is calculated from the images and the emission rates of these gases can be determined (see Part 2).

2 Instrumentation

The Scanning Infrared Gas Imaging System (SIGIS) used is comprised of an interferometer (OPAG 22, Bruker Daltonics, Leipzig, Germany), an azimuth-elevation-scanning mirror actuated by stepper motors, a telescope, a data and video processing and control system with a digital signal processor (DSP), a camera and a personal computer (Fig. 2). For the visualization of gas plumes, the scanning mirror is set sequentially to all positions within the field of regard (all pixels in the observation window). The size and direction of the field of regard and the spatial resolution (i.e. the angle between adjacent views) are variable. Each interferogram measured by the instrument is recorded by the DSP system where a Fourier transformation is performed and the spectrum is transferred to the PC. The spectrum is analysed on-line and the column densities are visualized as false color images laid over the calibrated video image. For each target compound, an image of the space-resolved Pearson's coefficient of correlation, the signal-to-noise ratio, the brightness temperature of the background and the difference between the temperature of the ambient air and the brightness temperature of the

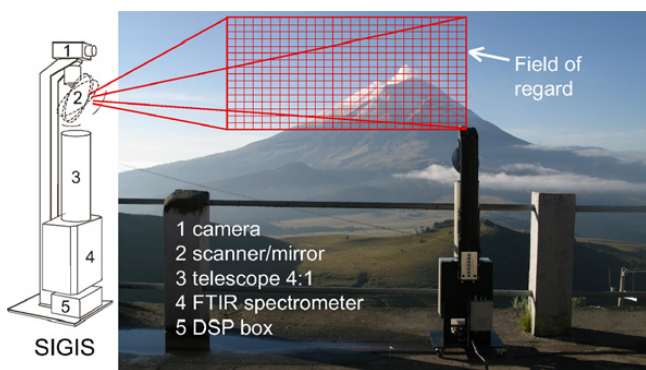


Fig. 2. (a) Schematics of the SIGIS construction with corresponding components and (b) illustration of the instrument scanning a 2-D image represented by the field of regard (red grid).

background are also produced. Simultaneous with the analysis and visualization of one interferogram by the DSP and the PC, the scanning mirror is set to move to the next position where a new interferogram is recorded. After the measurement of the field of regard is completed, the column densities of all directions in which a compound has been identified may be calculated and an additional false-color image is displayed (Harig et al., 2005).

For quantitative analyses of slant column densities, a radiometric calibration is necessary (Revercomb et al., 1988). The calibration was realized with spectra recorded at two different temperatures taken from a temperature-controlled black-body. There is a trade-off when choosing the spectral resolution in order to obtain sufficient information about the target and interference gases with higher resolution and looking to improve the signal-to-noise ratio and speed in the data acquisition gained when using the smaller resolution (Harig, 2004). We present two different data sets using spectral resolutions of 4 and 0.5 cm^{-1} . Fast measurements with the lower resolution allow for two-dimensional scans (consisting of typically 35×20 spectra) to be produced within 2 min and still average 5 interferograms per recorded spectrum (pixel). With the higher spectral resolution, 20 interferograms need to be averaged so that full 2-D-scans would take too long to be completed and would not reflect a snapshot of the volcanic plume. The higher resolution spectra are taken only in the spot-observation mode as described in Sect. 3.2.

The measurements presented in this work were done from the high-altitude Altzomoni site (19.12° N , 98.65° W , 4000 m a.s.l.) at a safe distance of 12 km from the crater.

3 Retrieval algorithms

3.1 Algorithm for the 4 cm^{-1} resolution

Passive remote sensing of gas clouds is based on the analysis of infrared radiation absorbed and emitted by the molecules.

Figure 1b illustrates the measurement set-up of the method. The radiation measured by the spectrometer contains the spectral signatures of the background in the field of view, the gas cloud, and the atmosphere. The propagation of radiation through the atmosphere is described by the theory of radiative transfer, Eq. (1).

$$L_1 = (1 - \tau_1) B_1 + \tau_1 [(1 - \tau_2) B_2 + \tau_2 L_3]. \quad (1)$$

In order to describe the basic characteristics of spectra measured by a passive infrared spectrometer, a simple model with three layers is used (Fig. 1b). Radiation (L_3) from the background (Layer 3), for example the sky (or a surface), propagates through the volcanic plume (Layer 2) and the atmosphere between the plume and the spectrometer (Layer 1). τ_1 , τ_2 and B_1 , B_2 describe the transmissions and the radiation due to thermal emissions (from Planck's-function) in these layers, respectively. The layers 1 and 2 are assumed homogeneous with regard to all physical and chemical properties within each layer. The radiation containing the signatures of all layers (L_1) is measured by the spectrometer and the spectra are analyzed by the GeDetekt software developed for the SIGIS (Harig et al., 2009). The reference spectra with different column densities along this path are calculated by the convolution of high resolution transmittance spectra calculated by FASCODE (Smith et al., 1978) using the HITRAN spectral compilation and an instrumental line-shape function. The spectra measured by passive remote sensing spectrometers contain both absorption and emission signatures of the target gas. Baseline shifts in the spectrum that exceed the signal of the target compound due to the radiance of the background and emission inside the spectrometer are also considered. The signatures of atmospheric trace gases, and in particular the signatures of ozone and water vapour, are often greater than the signatures of the target gases. Therefore, the algorithm is optimized to identify and quantify the compounds where the mentioned interference gases and baseline shifts are less sensitive.

The analysis is realized by the approximation of a measured spectrum with a linear combination of reference spectra, which have been converted to brightness-temperature $T_{\text{br}}(\tilde{\nu})$ ($\tilde{\nu}$: frequency in wavenumbers). $T_{\text{br}}(\tilde{\nu})$ is obtained by the inversion of Planck's function $B(\tilde{\nu}, T)$ assuming that the thermal radiation is given by the measured intensity of the radiation $L(\tilde{\nu})$, Eq. (2).

$$T_{\text{br}}(\tilde{\nu}) = \frac{h c \tilde{\nu}}{k} \left(\ln \left[\frac{2 h c^2 \tilde{\nu}^3}{L(\tilde{\nu})} + 1 \right] \right)^{-1}. \quad (2)$$

For the calculation of the slant-column densities, a plume temperature in the volcanic layer has to be estimated. For the analysis of spectra at 4 cm^{-1} taken on 16/17 November 2008 the value 275 K was used and for those taken on 28 May 2009 a temperature of 280 K was chosen. Although an exact value of the plume temperature is not known, the visualization and determination of molecular ratios between SiF_4 and SO_2 are

quite insensitive to the plume temperature as described by Love et al. (2000) and shown in Sect. 5.1.

An example of the retrieval results of SO₂ and SiF₄ are shown in Fig. 3. The regions used for the analyses of SO₂ and SiF₄ are 1050–1250 cm⁻¹ and 980–1080 cm⁻¹, respectively. The strong SO₂ ν₁-band located around 1150 cm⁻¹ can be clearly seen in the spectrum, while that of SiF₄ is weak and slightly larger than the noise in this case. When the fitting parameters from the continuum and other interference gases are removed (blue trace), the SiF₄ signal can more easily be identified.

The presence of ash in volcanic plumes can affect the analysis significantly preventing the possibility to quantify the column densities. The emission and absorption of the ash-particles act as a continuum in the spectra similar to that of a solid background like the cone of the volcano. In such cases an analysis using difference spectra (sky-plume) is not possible and a filter is introduced. The integrated intensity between 900 and 1000 cm⁻¹ is used to exclude all spectra which are above an empirical intensity-threshold of the received IR-radiation. The scheme works also to exclude the pixels in which the volcano or clouds are in the field-of-view so that more representative slant columns of the target gases and a corresponding SiF₄/SO₂ ratio can be obtained.

3.2 Algorithm for the 0.5 cm⁻¹ resolution

The instrument was designed for thermal emission spectroscopy at different resolutions. For the 0.5 cm⁻¹ resolution, the system was set to measure in “spot” mode, which means that it will measure continuously in one direction or it can alternatively switch between two or more directions (pre-defined spots). A new code to retrieve slant columns from individual thermal emission spectra at this resolution was developed. Using a higher resolution has the disadvantage of a lower S/N but it helps to separate absorption features of different gases better and might therefore lower systematic errors.

Just as for the lower resolution mode the atmosphere is divided also in 3 layers, each containing a number of relevant gases described by their partial columns and a mean temperature. The forward model thus is similar as the one described in Sect. 3.1., in Harig et al. (2009) and by Goff et al. (2001). The cross-sections are calculated in a preprocessing step using FASCODE with sufficient high resolution (no apodization) and on a fine grid. Depending on the width of the spectral window, a polynomial of order N is used to simulate the black-body radiation from aerosol, ash particles or water drops in the atmosphere and the volcanic plume.

The assumption of a temperature in each layer is required in the forward model. The vertical T-profile from the daily radiosonde launched in Mexico City and the US Standard atmosphere were used for the background layer and

we estimated the temperature $T_{\text{bg-layer}}$ with a weighted average using

$$T_{\text{bg-layer}} = \frac{\int T(z) \rho_{\text{O}_3}(z) B(T(z)) dz}{\int \rho_{\text{O}_3}(z) B(T(z)) dz}, \quad (3)$$

where $B(T(z))$ is the black-body radiation and $\rho_{\text{O}_3}(z)$ the density of the main gas emitting in that region (for example ozone in the SiF₄ retrievals). The foreground temperature is estimated from the instantaneous temperature measured at the observation site. The estimation of the temperature in the volcanic layer is discussed in Sect. 4. The forward model considers that the instrumental line-shape results from a physical triangular apodization with maximal optical path-difference (OPD) of 1.8 cm (Harig et al., 2005; Stremme et al., 2009).

The inversion is done using the optimal estimation approach (Rodgers, 1976) and because the forward model is not linear, a Levenberg-Marquard damping mechanism is added. For each parameter, an a priori value and its co-variance has to be chosen. The choice of the number of parameters, a priori values and constraints is critical. The foreground, volcanic and atmospheric background layers are assumed to be independent and a diagonal a priori covariance matrix was chosen. The S_e -matrix describes the noise in the spectrum but according to the work of von Clarmann et al. (2001), a generalized S_e -measurement-noise matrix enables the reduction of errors introduced by not fitted or poorly known parameter in the forward model.

The spectral region of 1080–1205 cm⁻¹ was used for the SO₂ retrieval and the cross-section were calculated using the HITRAN 2004 database (Rothman et al., 2005). The following temperatures were assumed for the event on 17 November 2008: 300 K (foreground), 280 K (volcanic layer) and 250 K (atmospheric background). A polynomial of order 4 was used to simulate the continuum of this broad spectral window and the gases SO₂, O₃, CO₂, CH₄, N₂O and H₂O are taken into account. SO₂ from urban origin is considered negligible at this altitude and was only allowed to adapt freely in the volcanic layer, while CO₂, CH₄, N₂O and H₂O are fitted in the foreground layer.

A large source of error in the quantitative determination of the SO₂ slant-columns is the interference of water vapor. For the 0.5 cm⁻¹ resolution the non-Voigt line-shape might be of minor importance, however, its strong variability and the presence of water in all three layers makes it difficult to simulate. Even if one could determinate the foreground water-column using the humidity measured in situ, it would be difficult to get rid of spectroscopic problems with the H₂O interference, especially with the intense water lines. Therefore, the spectrum was dewighted systematically using the water cross-section as presented in Fig. 4 and which, as mentioned above, is similar like the use of a generalized S_e -matrix (von Clarmann et al., 2001).

The SiF₄ cross-sections were calculated from a laboratory spectrum ($T = 300$ K, $P = 1000$ hPa, 55 ppm, 1 m, at

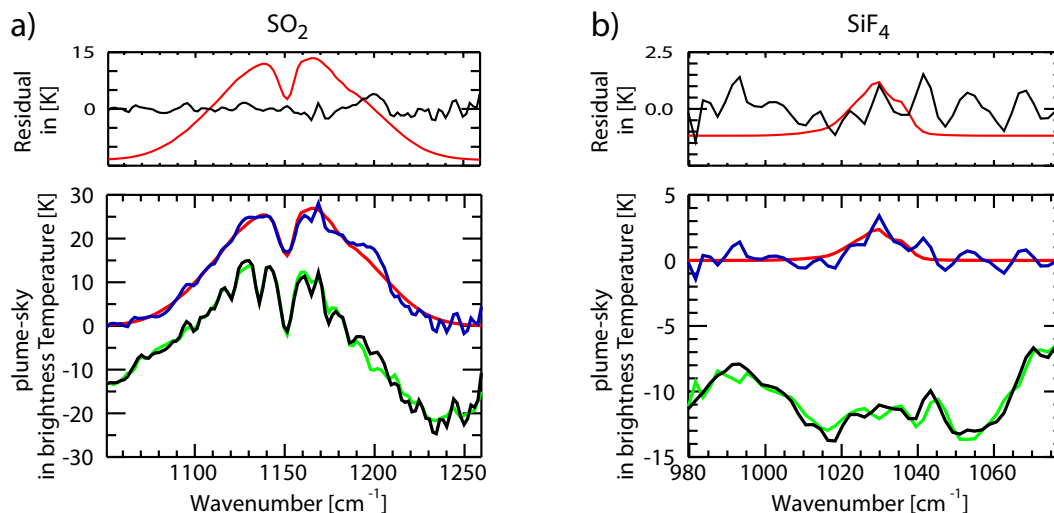


Fig. 3. Spectral regions where SO_2 (a) and SiF_4 (b) are retrieved at 4 cm^{-1} resolution. Lower plots: The difference of a plume spectrum and a reference-sky spectrum are shown in black and the corresponding fits in green. The same is plotted above for the spectra (blue) and fits (red) when all other fit parameters (continuum radiation and interference gases) are removed. Above: the residuals of the fits for each retrieval window.

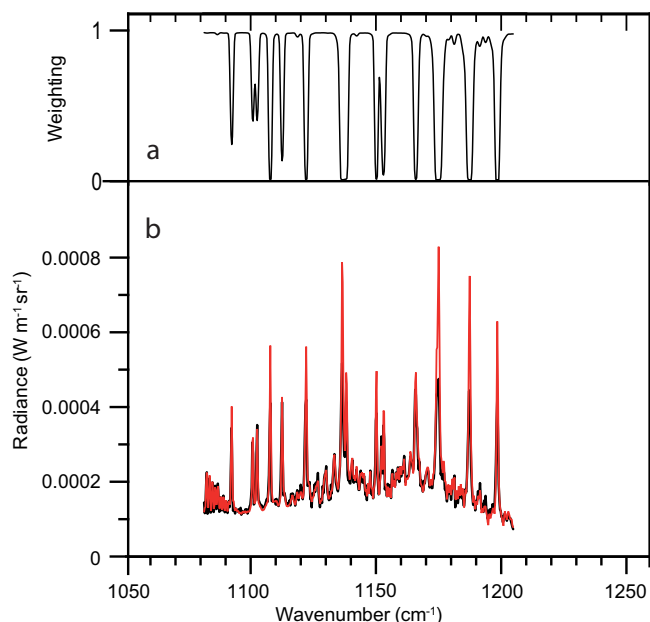


Fig. 4. Thermal emission spectrum (below) around the SO_2 ν_1 -band on 17 November 2008 at 17:45 LT. The black trace is the measured spectrum in the direction of (B) depicted in Fig. 1, and the red trace corresponds to the fitted simulation. The H_2O cross-section (above) is used for systematically deweighting the water lines in the analysis.

1.0 cm^{-1} resolution) from Hanst et al. (1996) which has also been used by Francis et al. (1996); Love et al. (1998); Mori et al. (2002). The same temperatures as for the SO_2 -retrieval were assumed for the three layers. In the chosen spectral

region, $1020\text{--}1040\text{ cm}^{-1}$, the gases SiF_4 , O_3 , CO_2 , CH_4 , N_2O and H_2O were forward simulated, but only SiF_4 , O_3 , CO_2 , H_2O and a polynomial of order 2 were fitted. Figure 5 shows the measured and simulated spectra with dominant O_3 structures, and a SiF_4 signature that is only slightly larger than the residual. As we will see in the results, this signal is sufficiently large to follow the evolution of a SiF_4 which is strongly correlated to SO_2 .

4 Validation of SO_2 and SiF_4 0.5 cm^{-1} retrievals from lunar absorption measurements

The results of SO_2 and SiF_4 slant columns retrieved from lunar absorption spectra (spot A in Fig. 1) are shown in Fig. 6. The analysis of the data was performed as from solar absorption spectra in Stremme et al. (2009). The measurements were taken on 17 November 2008 around 06:30 a.m. LST at when the moon had a zenith angle of 30° and an illumination fraction of 76%. The volcanic plume passed just above the observation site and it was possible to take absorption spectra for little less than an hour. As the thermal emission from the moon and that of the atmosphere including the volcanic plume have the same order of magnitude, background spectra just next to the moon were also recorded. These background spectra served rather to get slant columns in thermal emission mode since the plume was just above the measurement site. Figure 7 shows that one of the lunar background measurements (a thermal emission spectrum) was recorded near the maximum of the slant columns retrieved from lunar absorption. Therefore, it is possible to subtract an individual background obtained by linear interpolation from the thermal emission spectra recorded before and afterwards. Since

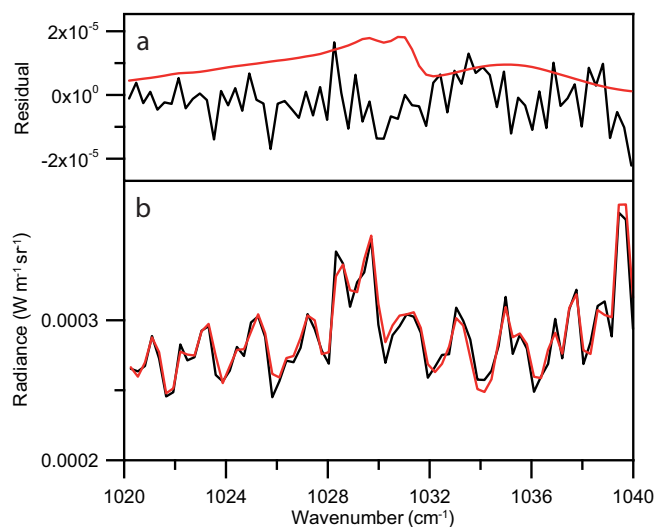


Fig. 5. Thermal emission spectrum (below) in the region used for analyzing SiF_4 . The black trace is the measured spectrum in the position of B depicted in Fig. 1, and the red trace corresponds to the fitted simulation. The fit residual (above) is shown in black together with a forward simulation of SiF_4 alone with the fitted result of $4.5 \times 10^{15} \text{ molec cm}^{-2}$.

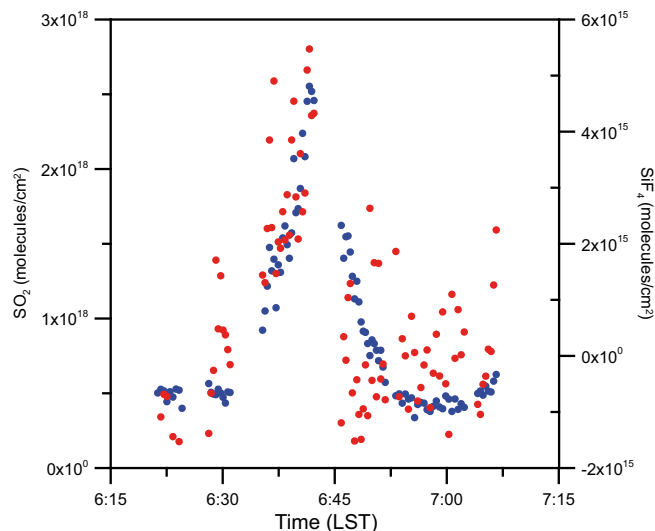


Fig. 6. Time-series of the SiF_4 (red) and SO_2 (blue) slant columns retrieved from lunar absorption spectra taken on 17 November 2008. Time is given in local time.

this subtraction eliminates most artifacts in the spectra which occur also from self emission of the instrument (Schreiber et al., 1996), the emission of the instrument is not taken into account in the forward model.

The first assumption of a volcanic plume temperature of 272 K lead to a systematic lower SO_2 column retrieved from thermal emission spectra than the temperature independent retrieval results from lunar absorption spectra (the blue triangle in Fig. 7. is the lunar absorption value interpolated to the

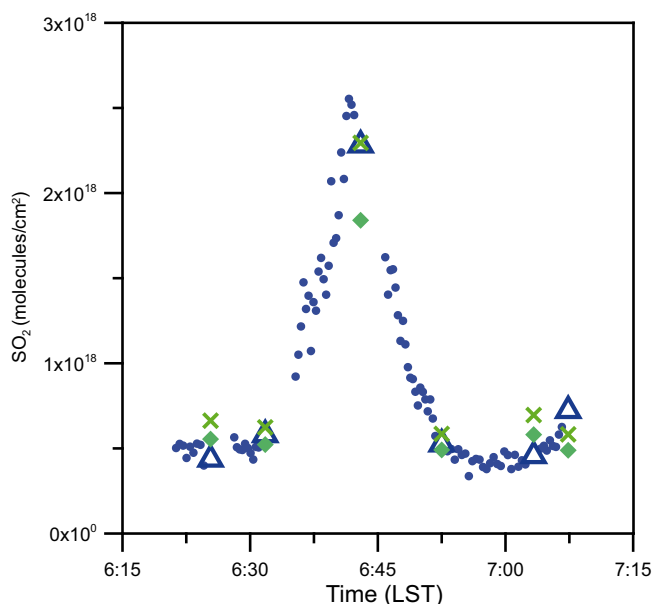


Fig. 7. Slant columns of SO_2 retrieved from lunar absorption spectra (blue) plotted together with SO_2 from thermal emission spectra at 0.5 cm^{-1} (green). The diamonds are results when a plume temperature is assumed to be 272 K and the crosses are after fitting the SO_2 columns to the lunar absorption value, giving a plume temperature of 266 K.

time of the thermal emission measurement). The results of the sensitivity study in Fig. 9 shows a temperature of 266 K, for which both SO_2 -slant columns are consistent. That is indicated by the green crosses (thermal emission) and blue triangle (interpolated lunar measurements) in Fig. 7. The plume temperature is a parameter which can be obtained from the comparison of both methods. The radiosonde at 17 November 2008, 06:00 a.m. L.T. at Mexico City registered a temperature of 265 K at 5000 m a.s.l., which was the approx. plume height. This result suggests that the volcanic plume seems to adapt rather fast to the temperature of the environment.

5 Errors and diagnostics

Random errors of the retrieved columns can be estimated from the scattering of the results (Figs. 8, 11 and 12). In the calculation of ratios, the random error obtained from the 95% confidence intervals is small if enough spectra are recorded. This error is used for all molecular ratios (SiF_4/SO_2) reported in this work and shown as vertical bars in Figs. 9 and 13. However, various parameters in the forward model affect the results systematically and have to be discussed to evaluate the results and to improve future measurements.

5.1 Sensitivity to plume temperatures

The assumed plume temperature has a strong impact on the estimated slant columns, and is normally not measured

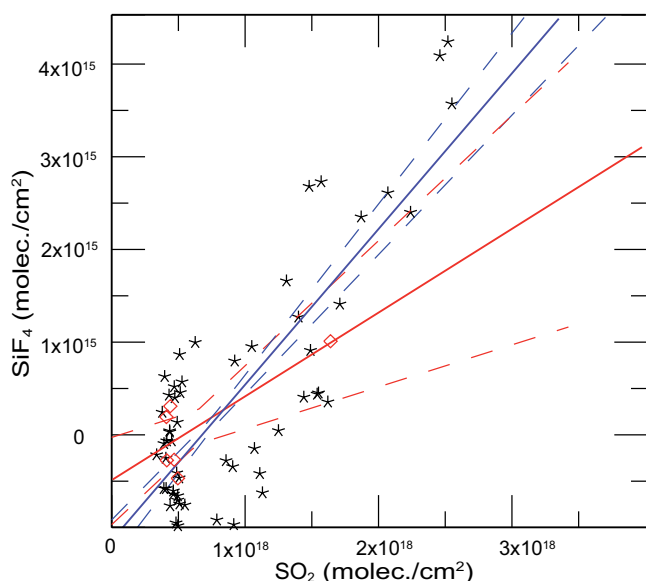


Fig. 8. Slant columns of SiF₄ retrieved from lunar absorption spectra (black) plotted together with SiF₄ from thermal emission spectra at 0.5 cm⁻¹ (red) against the corresponding SO₂ columns. Temperature of the plume is estimated to be 266 K (see, Fig. 7 and text). The molecule ratios are calculated from the linear fit and its error is indicated by the 95 % confidence interval.

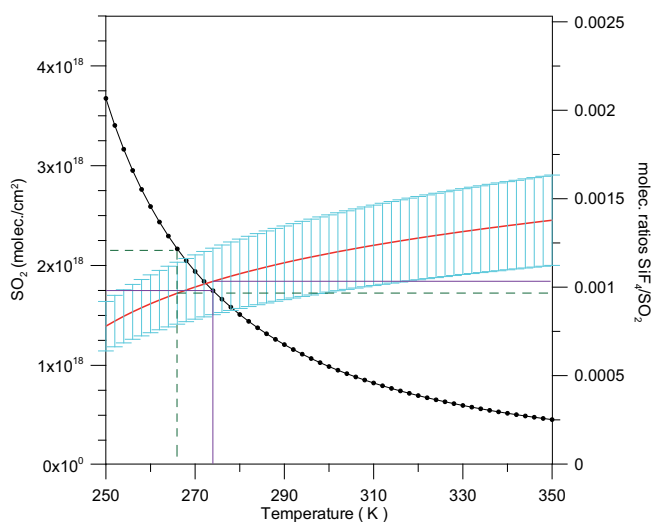


Fig. 9. Sensitivity of the retrieved SO₂ column to the estimated plume temperature (black points). The red line shows the resulting SiF₄/SO₂ molecular ratios as a function of chosen plume temperature. The ratios and its error are obtained from the slope of the linear fits of six thermal emission spectra taken at 0.5 cm⁻¹ resolution near the moon and between the lunar measurements (see, Figs. 7 and 8)

directly. Love et al. (2000) limited their analysis by using molecular ratios of the volcanic gases and not the absolute slant column amounts, which would be needed for estimating the flux. They mentioned that from their analy-

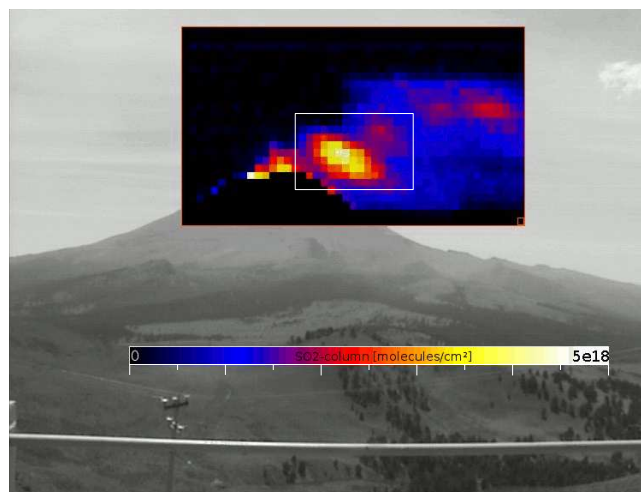


Fig. 10. A typical SO₂ plume from Popocatepetl volcano measured from the Altzomoni site on 17 March 2006. The slant column densities can be obtained with the on-line evaluation software after proper radiometric calibration and plume temperature estimation. The SO₂ amount of a single puff in the white rectangle corresponded to an estimated mass of (4 ± 1)t.

sis, the SiF₄/SO₂ ratio changes by less than 5 % if a 20 K higher volcanic plume temperature is assumed. This is confirmed from a sensitivity study performed from our results (see Fig. 9). Here it can be seen that although the changes in the retrieved slant columns can be rather large, the temperature dependence of the molecular ratio does not significantly change.

SO₂ and SiF₄ were analysed for this sensitivity study assuming different plume temperatures from a set of six thermal emission spectra of the volcanic plume taken some distance down-wind from the crater, close to the direction of the moon (spot A in Fig. 1). As the moon-absorption measurements (see Sect. 4) were performed at the same time and elevation angle, the volcanic-plume temperature could be estimated using the results from the sensitivity study and the moon-absorption quite accurately. This strategy is similar to using simultaneous COSPEC-measurements as described by Love et al. (2000), who used the SO₂ slant column from an independent technique for “calibrating” the thermal emission result. Other possibilities for estimating the temperature could be from strong saturated water lines or from the altitude of the volcanic-plume together with the assumption that it adopts the temperature of the environment at that altitude.

5.2 Plume inhomogeneity

The error discussed above considers the temperature of the plume to be homogeneous. However, the plume is inhomogeneous and dispersed over a wide area. The center in the field-of-view might not match the center of mass of the plume, and might change during the measurement. The

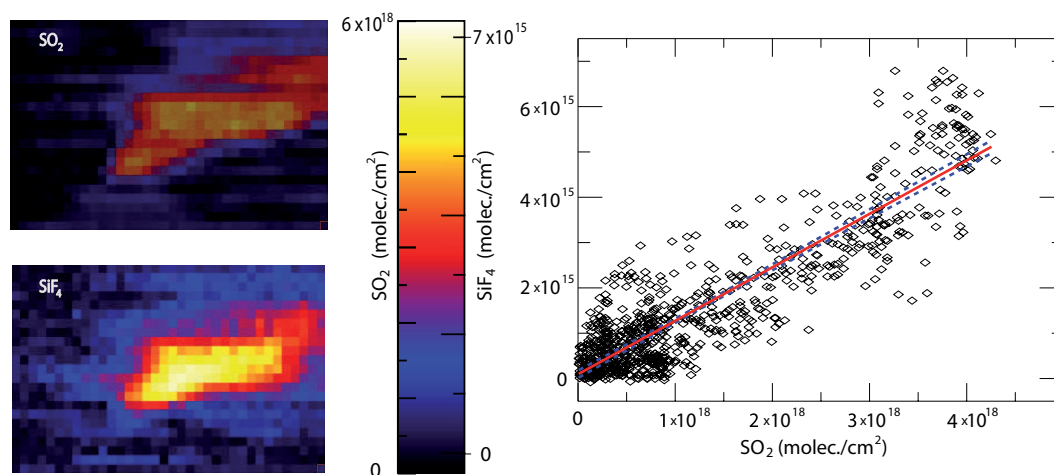


Fig. 11. Left panel: on-line analysis of the SO_2 and SiF_4 plumes displaying the retrieved slant columns in false-colored images. Difference spectra were calculated using the outermost left pixel as background and a temperature of 280 K was assumed for the evaluation. The sum of the slant columns within this window corresponds to 12 t of SO_2 and 24 kg of SiF_4 . Right panel: correlation between the column-densities of both gases in the scanned window resulting in a SiF_4/SO_2 ratio of $(1.80 \pm 0.034) \times 10^{-3}$.

Table 1. Sensitivity to calibration: study with lunar-background measurements assuming a temperature of 273 K of the volcanic plume. The calibration temperatures were 284.45 and 292.55 K.

perturbation		1	2	3	4
δ Temp. cold		+1	0	+1	-1
δ Temp. hot		0	+1	+1	+1
$\delta \text{SO}_2^{\text{max}}$	molec cm^{-2}	-0.30E+18	0.02E+18	0.02E+18	0.67E+18
$\delta \text{SO}_2^{\text{max}}$	%	-17.2	1.2	1.2	38.7
$\delta \text{SiF}_4^{\text{max}}$	molec cm^{-2}	0.18E+15	-0.20E+15	-0.018E+15	-0.14E+15
$\delta \text{SiF}_4^{\text{max}}$	%	12.5	-14.2	-1.2	-9.7
$\delta(\Delta \text{SO}_2)$	molec cm^{-2}	-0.180E+18	0.018E+18	0.018E+18	0.422E+18
$\delta(\Delta \text{SO}_2)$	%	-14.8	1.5	1.5	34.7
$\delta(\Delta \text{SiF}_4)$	molec cm^{-2}	-0.21E+15	0.34E+15	0.023E+15	0.66E+15
$\delta(\Delta \text{SiF}_4)$	%	-18.9	30.7	2.1	59.6
$\delta(\Delta \text{SO}_2/\Delta \text{SiF}_4)$	molec molec $^{-1}$	55.56	-244.50	-6.70	-170.07
$\delta(\Delta \text{SO}_2/\Delta \text{SiF}_4)$	%	5.09	-22.38	-0.61	-15.57

average temperature of a plume can be estimated from a range of altitudes covering the plume dispersing down wind. Even if the average plume temperature is well estimated, the temperature variations within the plume may cause uncertainties. The typical field-of-view presents a plume with a vertical thickness of around 2 km. If a lapse rate of 6.5 K km^{-1} is assumed the temperature difference between the lower and upper part and from the center of the plume would be $\pm 6.5 \text{ K}$. According to Fig. 9, this temperature difference would lead to an error of 16% in the slant column of SO_2 . However, the error in the molecular ratios would be smaller than 5%.

5.3 Radiometric calibration

One of the most important error sources of the experimental set-up used in this work is the radiometric calibration of the spectrometer. The calibration changes according to the temperature of the instrument and detector during measurements and a calibration every hour would be desired. Thus, the calibration itself might introduce errors, as the condition in the field was not always optimal for this procedure. The calibrations during the November/December 2007 campaign was not as frequent as in May 2009, although the available electrical power in the measurement site was not sufficient to raise the temperature of the black-body's resistance as high

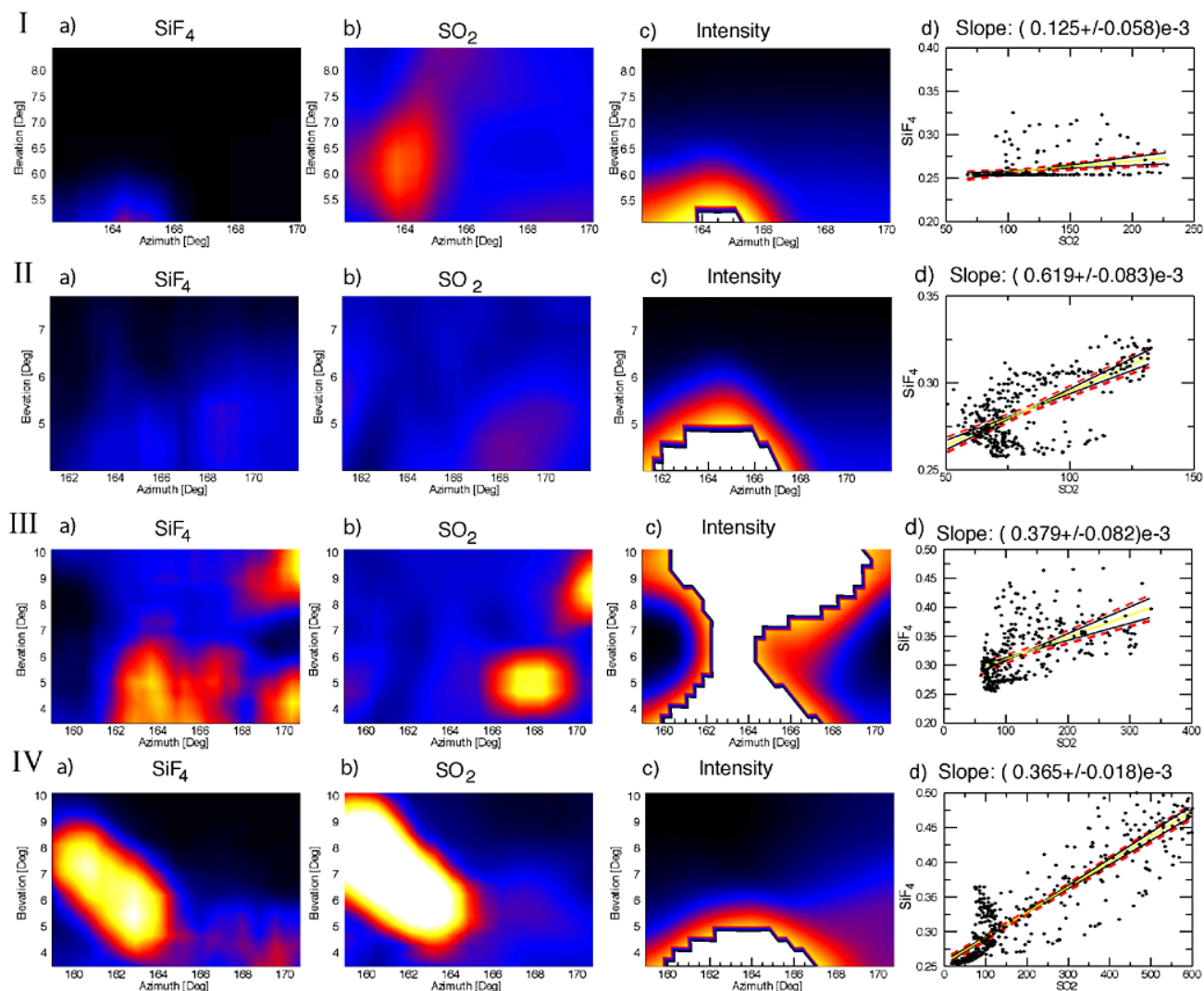


Fig. 12. Visualization of the (a) SO_2 and (b) SiF_4 slant columns retrieved at different times during the night of 16 to 17 November 2008 (colorbar for SiF_4 and SO_2 is the same as in Fig. 11). The integrated intensity around $900\text{--}1000\text{ cm}^{-1}$ is shown in (c) with colors in arbitrary units. The linear fits from the plots in (d) are calculated only from pixels with lower intensities – those with color in (c). A wind direction change is evident from the last row and one reference spectrum as clear sky was used for all the analysis (see video S.2 in the Supplement).

as in the previous study. The instrument was installed inside a building for the latter campaign looking for more stable temperatures and thus the conditions were better.

The error introduced by the calibration is evaluated assuming uncertainties in both the upper and lower temperatures of the black-body measurements. Both temperature errors could have the same or opposite signs. If we assume an error of 1 K, the effect in the slant columns and ratios can be calculated. The radiometric calibration also affects the slant columns retrieved from a clear-sky spectrum. Table 1 shows how the absolute slant-columns, the Δ slant-columns (plume-sky) and the calculated ratio between the ΔSiF_4 and SO_2 are affected. The error resulting from 1 K uncertainty in the temperatures of the black-bodies could lead to a 20 % error in the SO_2/SiF_4 ratios.

The different errors shown in Table 1 are important if the method is applied to determine (i) the absolute values of the slant column densities finally used for emission estimation or (ii) the differences in the slant columns (sky-plume) are retrieved to calculate molecular ratios. As there are different fitting parameters (continuum and interference gases) involved and the forward model is not linear, the error introduced through uncertainties in the calibration does not behave equally for all target gases. The table shows that molecular ratios could be affected by as much of 22 %, while a wrong calibration (1 K) might affect the column density by up to 60 % for SiF_4 and up to 35 % for SO_2 .

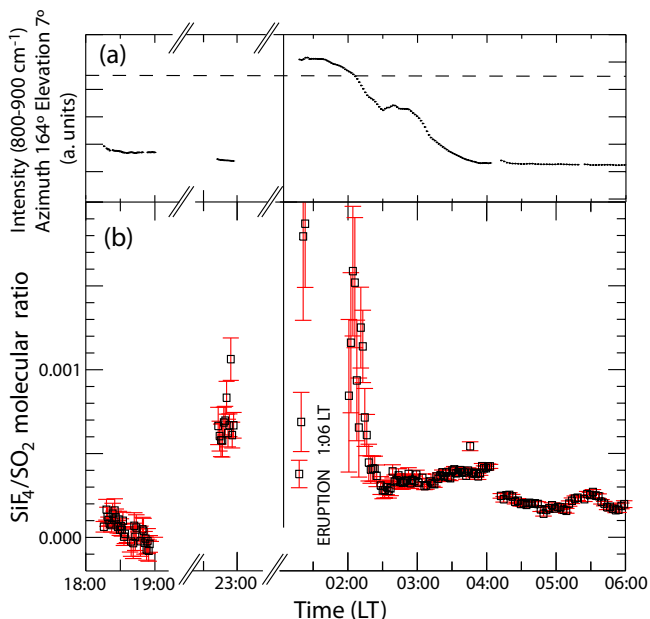


Fig. 13. Time-series of (a) the integrated radiation collected from above the crater and (b) the SiF_4/SO_2 molecular ratio (squares) before and after the eruptive event that took place between 01:06 and 01:45 LT of 17 November 2008. The dashed line indicates the threshold chosen to filter-out data for calculating molecular ratios.

5.4 Interference parameters

The a priori partial slant columns and a priori values used for the interference parameters are empirically adjusted. Errors in the interference gases or fitted parameters can therefore be large sources of error in the retrievals. The error analysis in optimal estimation is described by Rodgers (1990), Bowman et al. (2006) and Sussmann and Borsdorff (2007). An important tool in the error analysis is the Averaging-Kernel matrix which describes how a change in one parameter x_{true}^j affects the result related to another parameter x_{ret}^i . For the parameters which are retrieved with constraint, we define their average impact $\text{AI}_j^{\text{param}}$ on the target gas, for example for the SO_2 slant column, as:

$$\text{AI}_j^{\text{SO}_2} = A_j^{\text{SO}_2} \cdot \text{AVG}(x_{\text{ret}}^j - \text{a priori}) \quad (4)$$

The variance in the impact $\text{SI}_j^{\text{param}}$ is given by:

$$\text{SI}_j^{\text{SO}_2} = A_j^{\text{SO}_2} \cdot \text{STDEV}(x_{\text{ret}}^j) \quad (5)$$

Both quantities $\text{AI}_j^{\text{SO}_2}$ and $\text{SI}_j^{\text{SO}_2}$ help in the optimization process as they give insight in how the target gas reacts if the a priori value or the constraint of a certain parameter is changed. The retrieval of the target gas can be optimized efficiently by adjusting the interference parameters, a priori and constraint, so that the average of the volcanic gases in the clear-sky spectra (spot C in Fig. 1) is effectively zero, while

the target gases are almost unconstrained in the volcanic layer. The variance of the partly constrained interference parameters characterizes the retrieval as well. Both quantities $\text{AI}_j^{\text{SO}_2}$ and $\text{SI}_j^{\text{SO}_2}$ help in the optimization process and could indicate if something in the forward model is not well fitted or missing. The errors due to interference parameters can be minimized but not quantified in this way.

5.5 Uncertainty in the geometry

The measurements are taken from a rather large distance resulting in small scanning angles (maximal range was around 15°). This allows for geometrical approximations to be done and the slant columns can be thought of having constant separations at the plume distance. Also, the uncertainty in the observer-plume distance depends on both the direction and dispersion of the plume. Larger distances have proportionally smaller errors. To estimate the uncertainty rising from this distance, the evaluation is restrained to favourable conditions, in which the plume seems to propagate perpendicular to the viewing direction. Even in these selected cases the plume at some distance from the crater might have a displacement of half this distance towards or away from the measurement site. Typically the center of the recorded plume is around 2 to 3 km east or west of the crater, so that the distance to the center of the plume might be 11.5 ± 1.5 km. This represents a typical error of 13 % in the distance to the plume (r), leading to an error of 28 % in the integrated area ($A = \Delta\phi \cdot \Delta\theta \cdot r^2$), where ϕ and θ correspond to the azimuth and elevation angles. This error is irrelevant for slant column and molecular ratios, but it might be the major error source when determining the total amount and flux of a gas (see Part 2 of this paper). The total error for the mass calculation of a visualized puff of gas has an estimated value of $\approx 32\%$, which results from the slant column uncertainty ($\approx 16\%$) and the geometrical error ($\approx 28\%$) described here.

6 Results and discussion

Figure 10 shows a typical SO_2 plume from Popocatepetl volcano measured by thermal emission spectroscopy at 4 cm^{-1} . The SO_2 was retrieved according to the description made in Sect. 3.1, considering a plume temperature of 265 K. Various puffs are visible in the false-color image and the measured SO_2 slant columns can be integrated over one puff to estimate its SO_2 gas content. The puff in the right hand side of Fig. 10, for example, contains an estimated (4 ± 1) t of SO_2 when the area of the puff within the white rectangle is integrated, considering a distance of 12 km from the measurement site and a pixel size of 0.028° . The 2-D scans were continuously measured so that the plumes propagation could be animated over several hours (see animated videos in the Supplement).

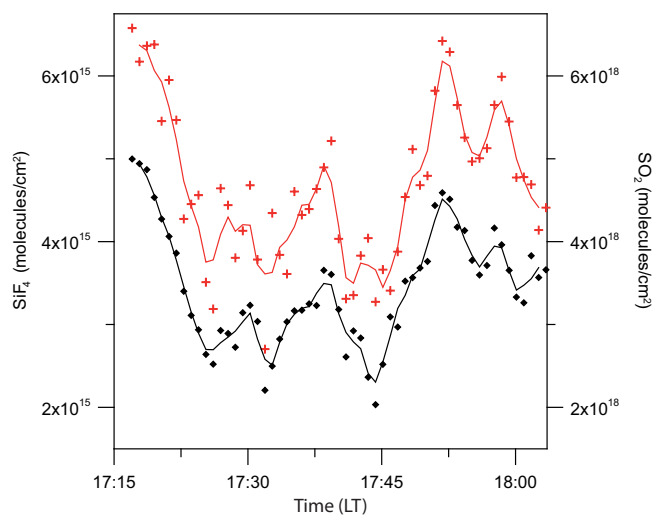


Fig. 14. Time series of the SO_2 (black diamonds) and SiF_4 (red crosses) slant columns obtained from thermal emission spectra recorded at 0.5 cm^{-1} resolution on 17 November 2008.

Volcanic SiF_4 slant columns were analysed from difference spectra at 4 cm^{-1} . At favorable conditions like on 28 May 2009, one 2-D scan which lasted around 1.5 min contains enough information to calculate the molecular ratio with a statistical error below 5 % (95 % confidence interval). The results of this scan are presented in Fig. 11. The SiF_4/SO_2 molecular ratio in this particular example is $(1.18 \pm 0.03) \times 10^{-3}$ and the corresponding SO_2 and SiF_4 amounts within the measured window are $(12 \pm 4)\text{ t}$ and $(24 \pm 8)\text{ kg}$, respectively. It is important to note that the near-horizontal viewing arrangement produces a strong interference with ozone and continuum radiation affecting the retrieved slant columns as well as the resulting absolute value of the molecular ratios. The presence of ash and clouds produce additional uncertainties and the reported ratios should therefore be treated carefully. However, it will be shown next that the relative changes in the measured ratios can be important parameters when related to the volcanic activity.

During the night 16/17 November 2008, an explosion occurred around 01:06 a.m. LST and large amounts of SO_2 and ash were emitted. The SiF_4 retrieval was performed from the difference spectra and still very close to the detection limit (see Sect. 3.1). To improve the signal-to-noise ratio in this event, the retrieved slant column densities of the nearest neighbors were averaged vertically and horizontally by a running average of 4. The results of a sequence are presented in Fig. 12. White areas where the integrated intensity are large (see Sect. 3.1) are filtered out clearly showing the presence of the ash-plume and the contour of the volcano in the third row, a few minutes after the explosion (01:18 a.m. LST). The corresponding animation of this sequence is presented as Supplement S.2.

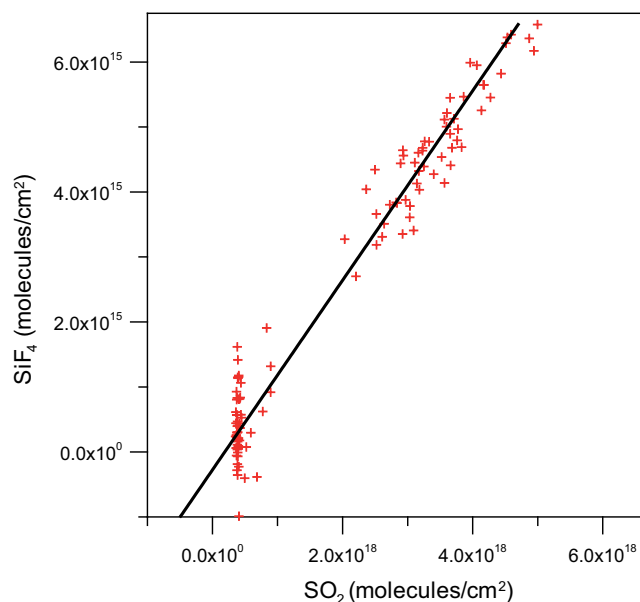


Fig. 15. SiF_4/SO_2 correlation plot from data in Fig. 10 including both plume and clear-sky spectra. Slope = $(1.4 \pm 0.07) \times 10^{-3}$.

A difference between the spatial distributions of SiF_4 and SO_2 would be interesting to analyze, as recent measurements at Fuego Volcano in Guatemala by Nadeau et al. (2011) with a UV-imaging system found SO_2 emitted through different vents. It is possible that just after the explosion, as seen in the third row of this sequence, the maximum of SiF_4 is propagated earlier towards the right border than SO_2 . Although a single snapshot does not provide sufficient arguments for making conclusions, it can be seen from the simultaneous plume animations that this instrument is capable of identifying differences in the spatial distribution of the gases (see S.2 in the Supplement).

In Fig. 13, the time series of both the integrated IR radiation collected just above the crater and the calculated SiF_4/SO_2 molecular ratios is presented. The time series of the integrated intensity (Fig. 13a) indicates the time and duration of the explosion. Only the values below the threshold, represented by the dashed line, were considered for calculating the gas ratios. One reference spectrum and one radiometric calibration, with a plume temperature assumed at 275 K, were used in the evaluation. These assumptions introduce uncertainties and therefore not the absolute but rather the relative behavior is interesting to observe. There is a clear increase in the SiF_4/SO_2 ratio not only after the eruption, but also a couple of hours before. The ratio then returns to low values several hours after the explosion.

Table 2. Results of the SiF₄/SO₂ ratios obtained from different measurement strategies.

Event	Mode	Resol. (cm ⁻¹)	SiF ₄ /SO ₂ × 10 ⁻³	R ²	N
17 November 2008 early morning	thermal emission image	4	0.39 ± 0.02	–	1 frame
17 November 2008 early morning	lunar absorption	0.5	1.68 ± 0.02	0.67	57
17 November 2008 early morning	thermal emission spot	0.5	0.90 ± 0.45	0.66	6
17 November 2008 morning	solar absorption ν ₁ + ν ₃	0.5	2.56 ± 0.30	0.65	213
17 November 2008 morning	solar absorption ν ₁	0.5	2.54 ± 0.26	0.66	156
17 November 2008 afternoon	thermal emission spot	0.5	1.40 ± 0.07	0.96	114
28 March 2009 early morning	thermal emission image	4	1.18 ± 0.03	0.80	828
28 March 2009 early morning	thermal emission spot	0.5	1.50 ± 0.18	0.69	110

A general behavior is deduced from the interpretation of Figs. 12 and 13. There is a low emission of gases several hours prior to the explosion. The SiF₄/SO₂ ratio starts to increase 2–3 h before, rises excessively during and just after the event and then drops to low values a few hours later. The emissions of both SO₂ and SiF₄, however, remain strong throughout the next day probably through open-venting.

Slant columns of SO₂ and SiF₄ at 0.5 cm⁻¹ were also recorded on 17 November 2008 (spot B in Fig. 1) during almost 1 h and are plotted in Fig. 14. The spectra were recorded ~16 h after the explosion with optimal conditions for measuring with thermal emission spectroscopy. A large variability observed in the retrieved slant columns is consistent with the puffs observed by Grutter et al. (2008). The SiF₄ and SO₂ columns are, however, changing synchronously. The Pearson's correlation of both columns including those from the clear sky (spot C in Fig. 1) results in a coefficient R² of 0.96 and a molecular ratio SiF₄/SO₂ of 0.00140 ± 0.00007 (Fig. 15). Errors are calculated with the 95 % confidence interval, assuming that the ratio is constant and errors in the SiF₄ retrieval are dominant. During the measurement period no significant change in the SiF₄/SO₂ ratio could be observed.

The results from various measurement periods, however, shows a significant variation in the SiF₄/SO₂ molecular ratios during quiescent degassing of Popocatepetl, Table 2. Not all measurements are equally reliable, as the geometry, meteorological conditions and calibration conditions might have differed. Table 2 differentiates between thermal emission measurements made in image mode, as shown in Figs. 11 and 12, and the spot mode as presented in Figs. 14 and 15. On the morning of 17 November 2008, a few spectra with volcanic gas were recorded near the moon when the measurement site was almost directly below the gas cloud. On 28 May 2009, measurements were recorded before sunrise using the scanning infrared system pointing above the crater while the instrument was located in the hut under more stable conditions.

The comparison of the molecular ratios presented in Table 2 between lunar absorption and thermal emission shows a difference of 0.00078 ± 0.0005. These measurements were

taken at the same time and the plume-temperature was adjusted according to the description presented in Sect. 4. As the systematic difference is only slightly larger than their uncertainty, the errors are estimated with the 95 % confidence interval, however, the dataset is based on only 6 measurements and in fact one plume measurement and 5 background measurements. As the interference gases and parameters play an important role in the SiF₄ retrievals, a greater set of measured spectra would be helpful. As the slant columns of SO₂ are consistent using the temperature of the environment at 5000 m a.s.l., we assume that there is a small systematic error in the retrieval of SiF₄. However, not sufficient evidence is available to infer which of both retrievals (thermal emission or absorption) remains slightly biased.

7 Conclusions

This work describes how a fully automatized scanning FTIR emission spectrometer can be used for plume visualization of volcanic gases, as well as continuous monitoring of emission ratios at favorable conditions. The instrument operation for thermal emission spectroscopy and the retrieval algorithms are described. The instrument can also be deployed to monitor other atmospheric relevant sources and in the case of continuous operation for volcanic surveillance, its automatized capability presents many benefits and opportunities allowing for:

- the detection of large column densities and molecular ratios of specific gases even during the night (with the possibility to warn with an alarm algorithm during an eruptive event),
- a visual representation of the individual volcanic gas plumes (with a large statistical significance from the increased data collection in various atmospheric and volcanic conditions),
- the identification of opportunities for taking solar or lunar absorption spectra of the plume (as when validating results from thermal emission measurements and performing specific studies like in Stremme et al., 2011),

- a detailed reanalysis of special events using individual optimized and adapted retrieval strategies.

The visualization of the SO₂ plume and its animation from longer sequences is presented (see the Supplement). The SiF₄ gas relevant for volcanic activity was simultaneously analyzed from the lower resolution spectra and it was possible to visualize its plume for the first time. SiF₄/SO₂ molecular ratios could be monitored from the sequential 2-D images at 4 cm⁻¹ with detected enhancements before and after an eruptive event. Alternatively, the 0.5 cm⁻¹ spectral resolution set in spot-observation mode just above the crater allowed for more information about the individual interferences to be acquired and an error estimation to be performed.

Down-wind plumes can be quantified such as in the false-color images of 28 May 2009 (Fig. 6), where the total SiF₄ and SO₂ contents were found to be (24 ± 8) kg and (12 ± 4) t, respectively, the latter being equivalent to the average SO₂ emission of Popocatepetl in 7 min. On 17 November 2008, there was an opportunity to measure the volcanic plume both by thermal emission and lunar absorption at the same time. The plume temperature for the thermal emission retrieval was adapted to match the slant columns of the lunar absorption result. The resulting temperature came out to be that of the environment at that particular altitude.

The large distance of 12 km to the crater and the near-horizontal field-of-view used in this study has some advantages, as the plume moved relatively slow and there was a possibility to monitor plumes in different altitudes and directions with almost the same elevation angle. However, that the atmospheric interference gases have large slant columns is a disadvantage. Therefore, the spectral signature of gases with smaller abundances, such as SiF₄, have small S/N ratios and can only be analyzed from difference-spectra.

The time series of SiF₄/SO₂ ratios, registered for the night of 16/17 November 2008, revealed a significant increase in SiF₄ before and during a Vulcanian-type eruption. The SiF₄/SO₂ ratio alone, however, might not be a reliable indicator for explosions and dome cooling, as both the S/F atomic ratio and the SiF₄/HF ratio are variable in the volcanic gas. An improvement of the spectrometer using for example a larger telescope together with a broader-range detector (MCT/InSb sandwich detector with bandpass-filters) would allow to simultaneously measure HCl at 2800 cm⁻¹ (Love et al., 2000; Gross et al., 2010). Multi-element detectors in the near future could also improve the acquisition speed and avoid the need of a scanning mirror. Also, as has been mentioned, the possibility of long-term monitoring with this technique would allow for gaining better emission statistics, which together with other parameters, wind conditions and seismic data, could provide new insights in the behavior of volcanic emission and activity.

Supplementary material related to this article is available online at:

<http://www.atmos-meas-tech.net/5/275/2012/amt-5-275-2012-supplement.zip>

Acknowledgement. We thank Claus Siebe from the Dept. of Vulcanology, Geophysics Inst.-UNAM for important discussions, Ivan Ortega for helping with the measurements, Alfredo Rodriguez from the workshop for technical support. We are also grateful with CONANP (the Izta-Popo National Park authorities) for hosting and supporting the field campaigns. DGAPA-UNAM (IN119310) is acknowledged for partial funding of this work. The referees are thanked for their comments which improved the quality of the manuscript

Edited by: J. Notholt

References

- Aiuppa, A.: Degassing of halogens from basaltic volcanism: Insights from volcanic gas observations, *Chem. Geol.*, 263, 99–109, doi:10.1016/j.chemgeo.2008.08.022, 2009.
- Bowman, K. W., Rodgers, C. D., Kulawik, S. S., Worden, J., Sarkissian, E., Osterman, G., Steck, T., Lou, M., Eldering, A., Shephard, M., Worden, H., Lampel, M., Clough, S., Brown, P., Rinsland, C., Gunson, M., and Beer, R.: Tropospheric Emission Spectrometer: Retrieval Method and Error Analysis, *IEEE Transactions on Geoscience and Remote Sensing*, 44, 1297–1307, doi:10.1109/TGRS.2006.871234, 2006.
- Burton, M. R., Oppenheimer, C., Horrocks, L. A., and Francis, P. W.: Diurnal changes in volcanic plume chemistry observed by lunar and solar occultation spectroscopy, *Geophys. Res. Lett.*, 28, 843–846, doi:10.1029/2000GL008499, 2001.
- Clarisse, L., Coheur, P. F., Prata, A. J., Hurtmans, D., Razavi, A., Phulpin, T., Hadji-Lazaro, J., and Clerbaux, C.: Tracking and quantifying volcanic SO₂ with IASI, the September 2007 eruption at Jebel at Tair, *Atmos. Chem. Phys.*, 8, 7723–7734, doi:10.5194/acp-8-7723-2008, 2008.
- Duffell, H., Oppenheimer, C., and Burton, M.: Volcanic gas emission rates measured by solar occultation spectroscopy, *Geophys. Res. Lett.*, 28, 3131–3134, doi:10.1029/2000GL012425, 2001.
- Francis, P., Chaffin, C., Maciejewski, A., and Oppenheimer, C.: Remote determination of SiF₄ in volcanic plumes: A new tool for volcano monitoring, *Geophys. Res. Lett.*, 23, 249–252, doi:10.1029/96GL00022, 1996.
- Francis, P., Burton, M. R., and Oppenheimer, C.: Remote measurements of volcanic gas compositions by solar occultation spectroscopy, *Nature*, 396, 567–570, doi:10.1038/25115, 1998.
- Goff, F., Love, S. P., Warren, R. G., Counce, D., Obenholzer, J., Siebe, C., and Schmidt, S. C.: Passive infrared remote sensing evidence for large, intermittent CO₂ emissions at Popocatepetl volcano, Mexico, *Chem. Geol.*, 177, 133–156, doi:10.1016/S0009-2541(00)00387-9, 2001.
- Gross, K. C., Bradley, K. C., and Perram, G. P.: Remote Identification and Quantification of Industrial Smokestack Effluents via Imaging Fourier-Transform Spectroscopy, *Environ. Sci. Technol.*, 44, 9390–9397, doi:10.1021/es101823z, 2010.

- Grutter, M., Basaldua, R., Rivera, C., Harig, R., Junkerman, W., Caetano, E., and Delgado-Granados, H.: SO₂ emissions from Popocatepetl volcano: emission rates and plume imaging using optical remote sensing techniques, *Atmos. Chem. Phys.*, 8, 6655–6663, doi:10.5194/acp-8-6655-2008, 2008.
- Halmer, M.: The annual volcanic gas input into the atmosphere, in particular into the stratosphere: a global data set for the past 100 years, *J. Volcanol. Geoth. Res.*, 115, 511–528, doi:10.1016/S0377-0273(01)00318-3, 2002.
- Hanst, P., Hanst, S., and Williams, G.: *Infrared Spectra for Quantitative Analysis of Gases*, QASoftDatabase, Infrared Analysis, Inc., Anaheim, CA, 1996.
- Harig, R.: Passive Remote Sensing of Pollutant Clouds by Fourier-Transform Infrared Spectrometry: Signal-to-Noise Ratio as a Function of Spectral Resolution, *Appl. Opt.*, 43, 4603–4610, doi:10.1364/AO.43.004603, 2004.
- Harig, R., Rusch, P., Dyer, C., Jones, A., Moseley, R., and Truscott, B.: Remote measurement of highly toxic vapors by scanning imaging Fourier-transform spectrometry, in: *Society of Photo-Optical Instrumentation Engineers (SPIE) Conference Series*, edited by: Jensen, J. O. and Thériault, J.-M., vol. 5995 of *Society of Photo-Optical Instrumentation Engineers (SPIE) Conference Series*, 316–327, doi:10.1117/12.631730, 2005.
- Harig, R., Rusch, P., Peters, H., Gerhard, J., Braun, R., Sabbah, S., and Beecken, J.: Field-portable imaging remote sensing system for automatic identification and imaging of hazardous gases, in: *Society of Photo-Optical Instrumentation Engineers (SPIE) Conference Series*, vol. 7475 of *Society of Photo-Optical Instrumentation Engineers (SPIE) Conference Series*, doi:10.1117/12.830627, 2009.
- Love, S. P., Goff, F., Counce, D., Siebe, C., and Delgado, H.: Passive infrared spectroscopy of the eruption plume at Popocatepetl volcano, Mexico, *Nature*, 396, 563–567, doi:10.1038/25109, 1998.
- Love, S. P., Goff, F., Schmidt, S. C., Counce, D., Pettit, D., Christensen, B., and Siebe, C.: Passive infrared spectroscopic remote sensing of volcanic gases: ground-based studies at White Island and Ruapehu, New Zealand, and Popocatepetl, Mexico, vol. 116 of *Geophys. Monogr.*, Am. Geophys. Union, 117–138, 2000.
- McGonigle, A. J. S.: Volcano remote sensing with ground-based spectroscopy, *Philos. T. Roy. Soc. Lond. A*, 363, 2915–2929, doi:10.1098/rsta.2005.1668, 2005.
- Mori, T., Notsu, K., Tohjima, Y., and Wakita, H.: Remote detection of HCl and SO₂ in volcanic gas from Unzen volcano, Japan, *Geophys. Res. Lett.*, 20, 1355–1358, doi:10.1029/93GL01065, 1993.
- Mori, T., Sato, M., Shimoike, Y., and Notsu, K.: High SiF₄/HF ratio detected in Satsuma-Iwojima volcano's plume by remote FT-IR observation, *Earth Planets Space*, 54, 249–256, 2002.
- Nadeau, P. A., Palma, J. L., and Waite, G. P.: Linking volcanic tremor, degassing, and eruption dynamics via SO₂ imaging, *Geophys. Res. Lett.*, 38, 1304–1308, doi:10.1029/2010GL045820, 2011.
- Notsu, K., Mori, T. G. G. I., Tohjima, Y., and Wakita, H.: Infrared spectral radiometer: a new tool for remote measurement of SO₂ of volcanic gas, *Geochem. J.*, 27, 361–366, 1993.
- Revercomb, H. E., Smith, W. L., Buijs, H., Howell, H. B., and Laporte, D. D.: Radiometric calibration of IR Fourier transform spectrometers - Solution to a problem with the High-Resolution Interferometer Sounder, *Appl. Opt.*, 27, 3210–3218, 1988.
- Rodgers, C. D.: Retrieval of Atmospheric Temperature and Composition From Remote Measurements of Thermal Radiation, *Rev. Geophys. Space Ge.*, 14, 609–624, 1976.
- Rodgers, C. D.: Characterization and error analysis of profiles retrieved from remote sounding measurements, *J. Geophys. Res.*, 95, 5587–5595, 1990.
- Rothman, L. S., Jacquemart, D., Barbe, A., Chris Benner, D., Birk, M., Brown, L. R., Carleer, M. R., Chackerian, C., Chance, K., Coudert, L. H., Dana, V., Devi, V. M., Flaud, J.-M., Gamache, R. R., Goldman, A., Hartmann, J.-M., Jucks, K. W., Maki, A. G., Mandin, J.-Y., Massie, S. T., Orphal, J., Perrin, A., Rinsland, C. P., Smith, M. A. H., Tennyson, J., Tolchenov, R. N., Toth, R. A., Vander Auwera, J., Varanasi, P., and Wagner, G.: The HITRAN 2004 molecular spectroscopic database, *J. Quant. Spectrosc. Ra.*, 96, 139–204, , 2005.
- Schreiber, J., Blumenstock, T., and Fischer, H.: Effects of the self-emission of an IR Fourier-transform spectrometer on measured absorption spectra, *Appl. Opt.*, 35, 6203–6209, 1996.
- Smith, H. J. P., Dube, D. J., Gardner, M. E., Clough, S. A., and Kneizys, F. X.: FASCODE: Fast Atmospheric Signature CODE (spectral transmittance and radiance), 1978.
- Stremme, W., Ortega, I., and Grutter, M.: Using ground-based solar and lunar infrared spectroscopy to study the diurnal trend of carbon monoxide in the Mexico City boundary layer, *Atmos. Chem. Phys.*, 9, 8061–8078, doi:10.5194/acp-9-8061-2009, 2009.
- Stremme, W., Ortega, I., Siebe, C., and Grutter, M.: Gas composition of Popocatepetl Volcano between 2007 and 2008: FTIR spectroscopic measurements of an explosive event and during quiescent degassing, *Earth Planet. Sc. Lett.*, 301, 502–510, doi:10.1016/j.epsl.2010.11.032, 2011.
- Sussmann, R. and Borsdorff, T.: Technical Note: Interference errors in infrared remote sounding of the atmosphere, *Atmos. Chem. Phys.*, 7, 3537–3557, doi:10.5194/acp-7-3537-2007, 2007.
- von Clarmann, T., Grabowski, U., and Kiefer, M.: On the role of non-random errors in inverse problems in radiative transfer and other applications, *J. Quant. Spectrosc. Ra.*, 71, 39–46, 2001.